A&A 388, 1062–1078 (2002)
DOI: 10.1051/0004-6361:20020587

Astronomy & Astrophysics

Molecular line scattering and magnetic field effects: Resolution of an enigma

S. V. Berdyugina[1], J. O. Stenflo[2], and A. Gandorfer[2]

[1] Astronomy Division, PO Box 3000, 90014 University of Oulu, Finland
[2] Institute of Astronomy, ETH Zentrum, 8092 Zurich, Switzerland

Received 11 February 2002 / Accepted 11 April 2002

Abstract. The linearly polarized solar spectrum that is produced by coherent scattering processes (also called "the second solar spectrum") is full of polarizing features due to molecular transitions, in particular from MgH and C_2. Their greatly different behavior in comparison with the observed polarization from atomic transitions has presented us with a new enigma: While the scattering polarization in atomic lines is very sensitive to magnetic fields via the Hanle effect and therefore exhibits polarization signatures that vary both spatially and with the solar cycle, the molecular polarization appears to be immune to the influence of magnetic fields. To clarify these issues we here develop a theoretical foundation for polarized molecular scattering, which can serve as a general tool for interpretations of the structures in the second solar spectrum. Intrinsic polarizabilities, line strengths, and effective Landé factors for the different transitions of the P, Q, and R branches of MgH and C_2 are calculated. While the intrinsic polarizabilities remain significant, the effective Landé factors are close to zero for the majority of the lines, in contrast to the behavior of atomic lines. This resolves the enigma and indicates how the molecular lines may serve as immutable reference lines against which the atomic lines can be gauged when trying to determine long-term, solar-cycle variations of the magnetic fields via the Hanle effect.

Key words. polarization – scattering – Sun: magnetic fields – molecular processes – techniques: polarimetric

1. Introduction

Coherent scattering on the Sun produces a wealth of linearly polarized spectral structures that are poorly correlated with the familiar spectral lines in the ordinary intensity spectrum. The spectrum seen in Stokes Q/I (degree of linear polarization) has therefore been referred to as the "second solar spectrum" (Ivanov 1991) because of its entirely different appearance and information contents. One of the big surprises when the richness of the second solar spectrum was first uncovered (Stenflo & Keller 1996, 1997) was the prominence of molecular contributions. While the molecular lines on the quiet Sun are very inconspicuous and barely visible, they stand out and in many spectral regions dominate the appearance of the second solar spectrum. The center-to-limb variation of their polarization amplitudes is steeper than for most of the atomic lines (Stenflo et al. 1997).

The first and successful attempt to theoretically understand the observed molecular scattering polarization for the non-magnetic case was done by Rao & Rangarajan (1999), who did radiative-transfer modelling of two Q-branch lines of MgH, at 5165.92 and 5168.14 Å, simultaneously fitting the observed Stokes I and Q/I profiles with the oscillator strength, inelastic collision rate, and depolarizing elastic collision rate as free parameters. An intrinsic molecular polarizability W_2 of 0.4 as derived from the J quantum numbers of the transition was used. W_2 is the fraction of the scattering processes that occur as polarizing dipole-type scattering (while the remaining fraction, $1-W_2$, represents isotropic, unpolarized scattering).

Recently Faurobert & Arnaud (2002) made an empirical determination of the W_2 polarizability factors for nine C_2 lines and two MgH lines. In contrast to previous observations they recorded with the THEMIS telescope the scattering polarization just *outside* the solar limb, where the radiation comes from an optically thin layer, which allows an interpretation without model-dependent radiative transfer. They found W_2 values of 0.41 and 0.46 for MgH, and between 0.13 and 0.26 for C_2. These values should however be considered as tentative until confirmed by independent observations, because off-limb observations are notoriously sensitive to spurious effects due to stray-light and seeing (cf. Keller & Sheeley 1999). As we will see, their results agree for MgH with the theory presented in

Send offprint requests to: J. O. Stenflo,
e-mail: stenflo@astro.phys.ethz.ch

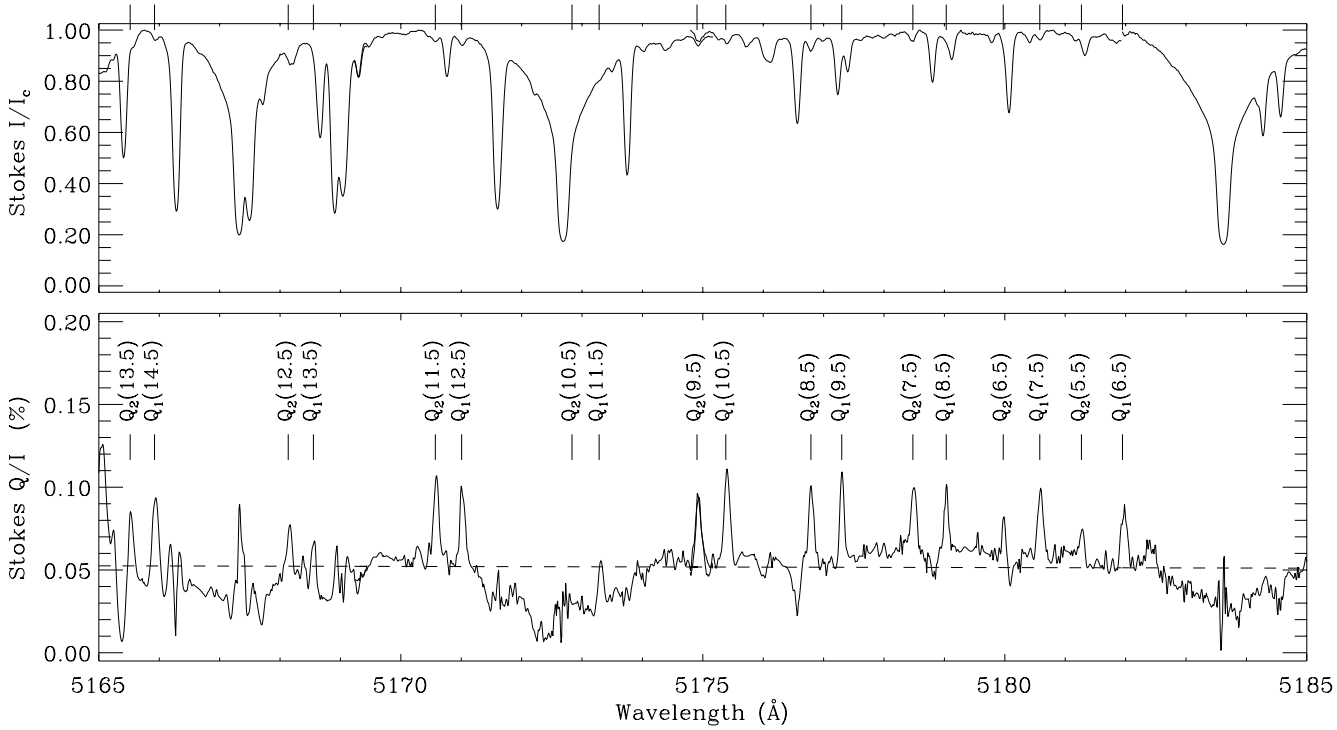

Fig. 1. 20 Å section from the Atlas of the Second Solar Spectrum (Gandorfer 2000) showing polarizing molecular lines from the Q branch of MgH. The J quantum number, which is the same for the lower and upper levels in the case of Q branch lines, is given in brackets after the identification. The atlas was recorded 5 arcsec inside the limb of the quiet Sun (at $\mu = 0.1$, where μ is the cosine of the heliocentric angle) with ZIMPOL (Zurich Imaging Polarimeter, cf. Povel 2001) at IRSOL (Istituto Ricerche Solari) in Locarno, Switzerland. The fractional linear polarization (Stokes Q/I) is defined to be positive when the plane of polarization is parallel to the nearest solar limb. The dashed line marks the level of the continuum polarization according to the theory of Fluri & Stenflo (1999). Since the zero point of the Q/I scale could not be determined to the same precision as the relative Q/I scale, it was chosen so that approximate agreement between the observed and theoretical continuum polarization was obtained. This procedure also applies to Figs. 9, 10, and 12 below.

the present paper, but for C_2 they disagree by a factor of two.

Magnetic fields influence the scattering polarization via the Hanle effect. The main effect when observing near the Sun's limb is Hanle depolarization, leading to reduced polarization amplitudes when magnetic fields are present. Due to this, the appearance of the second solar spectrum varies not only spatially, with the location on the Sun, but also temporally, with the phase of the solar cycle. Due to their different sensitivities to the Hanle effect, different spectral lines are affected to different degrees by the Hanle effect. This differential Hanle effect can be used for more model-independent diagnostics of spatially unresolved magnetic fields in parameter regimes not accessible with the ordinary Zeeman effect, e.g. weak, turbulent fields (Stenflo et al. 1998).

One striking and enigmatic feature found for the differential Hanle effect is that while the atomic lines exhibit large fluctuations of their depolarization factor, the molecular lines appear to be immune to the Hanle effect. When for instance comparing the Atlas of the Second Solar Spectrum (Gandorfer 2000) that was recorded near solar activity maximum with corresponding spectral sections recorded in 1995 near activity minimum, we find the same amplitudes for the molecular lines, while the atomic lines generally have substantially smaller amplitudes, and some depolarize the continuum rather than stand out above it. Figure 1 shows an example of a section of the Atlas with identifications of Q branch lines of MgH.

In addition to the 1-D Q/I spectra from the Atlas recordings at IRSOL (Locarno) that we use as examples in the present paper we have performed vector polarimetric imaging of all four Stokes parameters (I, Q/I, U/I, V/I) in different magnetic regions on the Sun. These recordings (still unpublished) show pronounced signatures of both the Zeeman and Hanle effects with large spatial fluctuations along the spectrograph slit, like the Stokes recordings published for the Na I D_2 and D_1 lines (Stenflo et al. 2001), but these fluctuations are only present for the atomic lines. Both the Zeeman and Hanle effect are absent in the prominent MgH and C_2 molecular lines, which appear immune to the influence of magnetic fields.

The aim of the present paper is to present a theoretical foundation for the interpretation of molecular lines in the second solar spectrum and to resolve the enigmatic, contrasting behavior between atomic and molecular

lines: Why are the molecular lines strongly polarizing while at the same time being immune to magnetic fields?

2. Polarizabilities of scattering transitions

2.1. Atomic case

Radiative scattering can be regarded as a two-stage process: radiative absorption followed by spontaneous emission. If the initial and final levels of a scattering process are the same, we speak of Rayleigh scattering, while if they are different we are dealing with Raman scattering. We use the notation J for the total angular momentum quantum number of an atomic state, and μ or m for the magnetic quantum numbers of a substate. Indices a, b, and f are used to mark if a substate is an initial, intermediate, or final state of the scattering process. If we let index β symbolize the polarization state of the incident photons, α that of the scattered photons, then the complex scattering amplitude from the initial to the final substate is given by the Kramers-Heisenberg dispersion formula (Stenflo 1994, hereafter S94, pp. 121–122)

$$w_{\alpha\beta} \sim \sum_b \frac{\langle f|\hat{\boldsymbol{r}}\cdot\boldsymbol{e}_\alpha|b\rangle\langle b|\hat{\boldsymbol{r}}\cdot\boldsymbol{e}_\beta|a\rangle}{\omega_{bf}-\omega-i\gamma/2}\,, \tag{1}$$

where the sum is taken over all intermediate substates with quantum numbers J_b and m. Through this sum the coherent superposition of both the different Zeeman sublevels m and of the different total angular momentum states J_b are taken into account. ω is the frequency of the scattered radiation, $\hbar\omega_{bf}$ the energy difference between the excited and final states, and γ the damping constant that accounts for the broadening of the excited state, while the initial state is assumed to be infinitely sharp. $\hat{\boldsymbol{r}}$ is the position operator, which is proportional to the dipole moment operator, and $\boldsymbol{e}_{\alpha,\beta}$ are the unit polarization vectors.

To describe the transformation of the incident to the scattered Stokes vector, we form the Mueller scattering matrix $\boldsymbol{M}$ as follows:

$$\boldsymbol{M} = \boldsymbol{T}\boldsymbol{W}\boldsymbol{T}^{-1}, \tag{2}$$

where $\boldsymbol{T}$ and $\boldsymbol{T}^{-1}$ are purely mathematical transformation matrices without physical contents (S94, p. 41). The elements of the radiation coherency matrix $\boldsymbol{W}$ are formed by the products of the scattering amplitudes $w_{\alpha\beta}$ in Eq. (1):

$$\boldsymbol{W} = \boldsymbol{w}\otimes\boldsymbol{w}^*, \tag{3}$$

if the relative populations of the initial magnetic substates μ_a are assumed to be equal (no initial-state atomic polarization). Since $w_{\alpha\beta}$ is a tensor, the tensor product is used (S94, p. 39).

The polarizability W_2 of a scattering transition represents the fraction of the scattering processes that behave like dipole-type (polarizing) scattering, while the remaining fraction $1-W_2$ behaves like isotropic, unpolarized scattering (S94, p. 183). W_2 is expressed via the elements of the $\boldsymbol{W}$ matrix and, hence, in terms of the amplitudes $w_{\alpha\beta}$. Therefore, in order to calculate W_2, we need to clarify first the meaning of the matrix elements $\langle f|\hat{\boldsymbol{r}}\cdot\boldsymbol{e}_\alpha|b\rangle$ and $\langle b|\hat{\boldsymbol{r}}\cdot\boldsymbol{e}_\beta|a\rangle$.

The scalar products between the position operator and the linear unit polarization vectors give rise to the geometrical factors $\varepsilon_q^{\alpha*}$ and ε_q^{β} (S94, p. 48) through

$$\hat{\boldsymbol{r}}\cdot\boldsymbol{e}_\alpha = \sum_q \hat{r}_q\,\varepsilon_q^{\alpha*}. \tag{4}$$

These factors are formed from the complex spherical vectors $\boldsymbol{e}_q$ through $\varepsilon_q^{\alpha*} = \boldsymbol{e}_q\cdot\boldsymbol{e}_\alpha$, where $q = 0, \pm1$. Thus

$$\langle f|\hat{\boldsymbol{r}}\cdot\boldsymbol{e}_\alpha|b\rangle = \langle J_f\mu_f|\sum_q \hat{r}_q\,\varepsilon_q^{\alpha*}|J_b m\rangle\cdot \tag{5}$$

However, since $q = \mu_f - m$, only one component of the sum contributes, so that

$$\langle f|\hat{\boldsymbol{r}}\cdot\boldsymbol{e}_\alpha|b\rangle = \langle J_f\mu_f|\hat{r}_q|J_b m\rangle\,\varepsilon_q^{\alpha*}. \tag{6}$$

Similarly, for the second amplitude, we obtain:

$$\langle b|\hat{\boldsymbol{r}}\cdot\boldsymbol{e}_\beta|a\rangle = \langle J_a\mu_a|\hat{r}_{q'}|J_b m\rangle^*\,\varepsilon_{q'}^{\beta}\,, \tag{7}$$

where $q' = \mu_a - m$.

The matrix elements in the above expressions may be expanded via the Wigner-Eckart theorem (S94, p. 145):

$$\langle J_f\mu_f|\hat{r}_q|J_b m\rangle = (-1)^{J_b+\mu_f+1}\sqrt{2J_f+1} \times\begin{pmatrix} J_b & J_f & 1\\ -m & \mu_f & -q\end{pmatrix}\langle J_f||\hat{\boldsymbol{r}}||J_b\rangle, \tag{8}$$

$$\langle J_a\mu_a|\hat{r}_{q'}|J_b m\rangle^* = (-1)^{J_b+\mu_a+1}\sqrt{2J_a+1} \times\begin{pmatrix} J_b & J_a & 1\\ -m & \mu_a & -q'\end{pmatrix}\langle J_a||\hat{\boldsymbol{r}}||J_b\rangle^*, \tag{9}$$

where the reduced matrix elements $\langle J_f||\hat{\boldsymbol{r}}||J_b\rangle$ and $\langle J_a||\hat{\boldsymbol{r}}||J_b\rangle^*$ can be directly related to the oscillator strengths of the transitions f_{fb} and f_{ab} (S94, pp. 192 and 199):

$$\langle J_f||\hat{\boldsymbol{r}}||J_b\rangle \sim (-1)^{r_{fb}}\sqrt{f_{fb}}\,, \tag{10}$$

$$\langle J_a||\hat{\boldsymbol{r}}||J_b\rangle^* \sim (-1)^{r_{ab}}\sqrt{f_{ab}}\,. \tag{11}$$

Here, r_{fb} and r_{ab} are even or odd integers depending on the quantum numbers L, S and J.

Thus, finally, we obtain the expanded expression of the scattering amplitude (S94, p. 174; Stenflo 1998):

$$w_{\alpha\beta} \sim \sum_{J_b,m}(-1)^{r_{ab}+r_{fb}}\sqrt{f_{ab}f_{fb}}\sqrt{(2J_f+1)(2J_a+1)} \times\begin{pmatrix} J_b & J_f & 1\\ -m & \mu_f & -q\end{pmatrix}\begin{pmatrix} J_b & J_a & 1\\ -m & \mu_a & -q'\end{pmatrix} \times(-1)^{q-q'}\Phi_{m\mu_f}\,\varepsilon_q^{\alpha*}\varepsilon_{q'}^{\beta}\,, \tag{12}$$

where

$$\Phi_{m\mu_f} = \frac{2/i}{\omega_{m\mu_f}-\omega-i\gamma/2} \tag{13}$$

is the normalized profile function, and

$$\omega_{m\mu_f} = (E_m - E_{\mu_f})/\hbar = \omega_{bf} + (g_b m - g_f \mu_f)\,\omega_{\rm L} \quad (14)$$

is the frequency of the transition between the magnetic sublevels m amd μ_f expressed via the Landé factors g_b and g_f of the intermediate and final J-states. $\omega_{\rm L}$ is the Larmor frequency.

2.2. Molecular case

Extending the theory of radiative scattering from atoms to diatomic molecules implies a basic change in the symmetry of the system – from the spherical symmetry of an atom to the axial symmetry of a diatomic molecule. The axial symmetry introduces a direction in which the total electronic orbital momentum and spin can be spatially quantized. Furthermore, a third angular momentum appears due to molecular rotation. Therefore the total angular momentum of a diatomic molecule is produced by three angular momenta and depends on how strongly they interact with each other. One can distinguish between a few coupling schemes for the three momenta with respect to how they combine with each other and the so-called internuclear axis. Independent of the coupling scheme, the total angular momentum quantum number conserves its values and is therefore always a good quantum number (assuming that there are no or only weak external perturbations, like from an external magnetic field). Because of this, molecular Zeeman sublevels are like atomic sublevels characterized by the quantum numbers J and m, the total angular momentum and its magnetic projection. Therefore radiative scattering in lines of diatomic molecules is generally described by the same expressions as given for the atomic case in Sect. 2.1. The difference appears only in calculations of the line oscillator strength, the Landé factors and the sign of the interference terms, i.e., in r_{ab} and r_{fb}, all of which also depend on the electronic quantum numbers that have no analogs in the atomic case. Leaving these parameters for the next section and the Appendix, let us here consider the main question of the polarizability of molecular scattering transitions when no interference is involved.

Since all the molecular lines considered here are weak without significant dispersion wings, interference will only be of significance between transitions with the same initial and final states, when the separation between the excited states is of the same order as the damping width, or smaller. This is not the case for the majority of the lines considered here. Although such interference can be neglected in the present work, we present the theory for it in the Appendix for the sake of completeness, to serve as a foundation for future applications.

As was noted in Sect. 2.1, the linear polarizability W_2 of a scattering transition is expressed through the elements of the matrix $\boldsymbol{W}$, which are functions of the quantum numbers J_a, J_b, and J_f. Due to the selection rule $\Delta J = 0, \pm 1$, however, the complicated expressions for W_2 can be reduced to simple ones for both Rayleigh and Raman scattering. The three sequences of transitions with $\Delta J = -1, 0, +1$ form, respectively, P, Q, R rotational branches. In the Rayleigh scattering case, when $J_f = J_a = J$ and $\Delta J = J_b - J$, the absorption and subsequent emission occur in the same branch line. The polarizability of these scattering transitions is as follows (S94, p. 188–189):

$$W_2(\mathrm{P}\rightarrow\mathrm{P}) = \frac{(J-1)(2J-3)}{10J(2J+1)}, \quad (15)$$

$$W_2(\mathrm{Q}\rightarrow\mathrm{Q}) = \frac{(2J-1)(2J+3)}{10J(J+1)}, \quad (16)$$

$$W_2(\mathrm{R}\rightarrow\mathrm{R}) = \frac{(J+2)(2J+5)}{10(J+1)(2J+1)}. \quad (17)$$

In the Raman scattering case, the absorption occurs in one branch and the emission in another. This case is exhausted by three transition types with $J_a < J_f$. Denoting again $J_a = J$, one obtains:

$$W_2(\mathrm{Q}\rightarrow\mathrm{P}) = -\frac{2J-1}{10(J+1)}, \quad (18)$$

$$W_2(\mathrm{R}\rightarrow\mathrm{Q}) = -\frac{2J+5}{10(J+1)}, \quad (19)$$

$$W_2(\mathrm{R}\rightarrow\mathrm{P}) = \frac{1}{10}. \quad (20)$$

All the cases when $J_a > J_f$ can always be converted to one of the cases above by reversing the direction of scattering, e.g., $W_2(\mathrm{P}\rightarrow\mathrm{R}) = W_2(\mathrm{R}\rightarrow\mathrm{P})$, etc.

Although these expressions are formally identical to the expressions obtained for the atomic case, their physical meaning is quite different. In the case of atoms, a single line corresponds to a single electronic transition, and the polarization of the line is unambiguously determined by the quantum numbers of the electron levels involved in the scattering process. In the case of molecules, a single electronic transition leads to the appearance of lines with different states of polarization (all the lines in R, Q, and P branches in many vibrational bands). This happens because there is a difference of several orders of magnitude between the lifetime of an excited electronic state and the period of molecular rotation: while a molecule is in an excited state, it will execute an extremely large number of rotations (as well as a large number of vibrations, which however do not affect the polarization).

In Fig. 2 the polarizability W_2 for the rotational branches is plotted for the Rayleigh scattering case and for the range of J numbers that are typical for molecular lines observed in the solar spectrum. It is interesting to note that the Q branch lines have four times larger polarizability for high J numbers. W_2 rapidly increases and approaches the asymptotic value 0.4 for $J > 7.5$. The opposite behaviour is seen for R branch lines, whose polarizability rapidly decreases and approaches from above

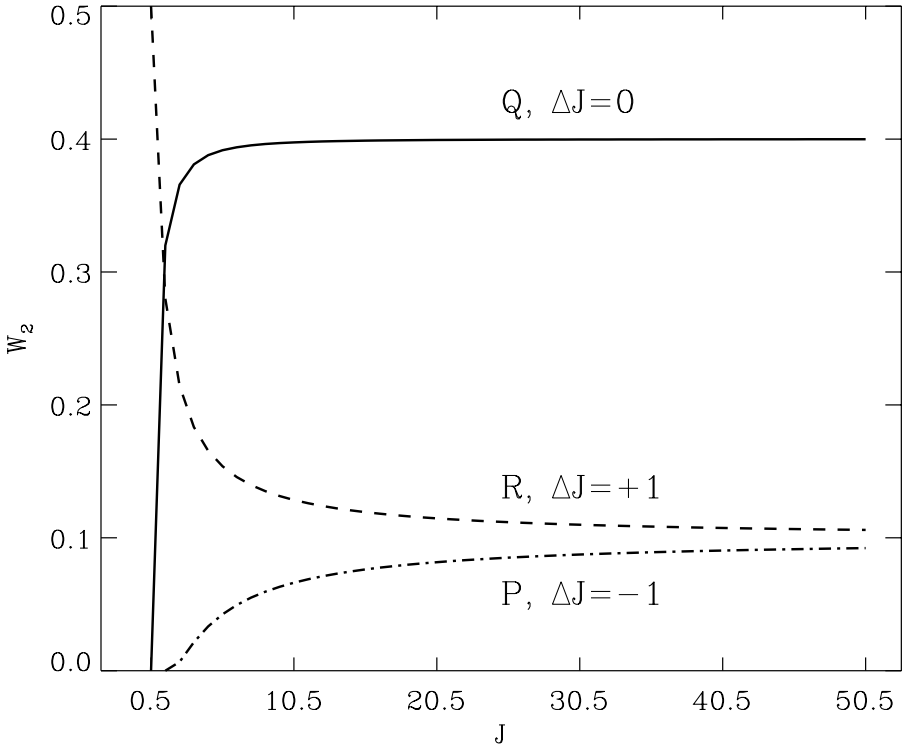

Fig. 2. The intrinsic polarizability W_2 for Rayleigh scattering in molecular lines for the P, Q, R rotational branches.

the asymptotic value 0.1. The same asymptotic value is reached from below for P branch lines, whose polarizability is the lowest, only between 0 and 0.1. The asymptotic limits for the polarizability with increasing rotation, i.e., with J number, have a simple classical interpretation (Feofilov 1961). Absorption and emission in lines of P and R branches may, in this limit, be described in terms of linear oscillators that are aligned with the molecular axis and therefore rotate together with it. In contrast, the processes in Q branch lines can be described in terms of oscillators that are aligned with the rotational axis of the molecule, i.e., perpendicular to the molecular axis.

In Fig. 3 the polarizability W_2 is plotted for the Raman scattering case. Here only two types of scattering transitions are important, namely Q $\rightarrow$ P and R $\rightarrow$ Q for $J_a < J_f$ (or correspondingly P $\rightarrow$ Q and Q $\rightarrow$ R for $J_a > J_f$). The polarizability of these transitions vary with J to rapidly approach the asymptotic value -0.2, starting from either 0.0 or -0.4. The significant difference with respect to the Rayleigh scattering case is that W_2 is negative. This means for instance that incoming light, which is linearly polarized perpendicular to the scattering plane, becomes polarized parallel to the scattering plane when emerging from the scattering event (S94, p. 189). Thus Raman scattering may reverse the state of the linear polarization, in contrast to Rayleigh scattering.

Let us finally note that the above polarization properties of the rotational branches are the same for all types of electronic transitions and all vibrational bands of diatomic molecules as long as J is a good quantum number.

3. Molecular Landé factors and intensity factors

The axial symmetry of a diatomic molecule causes the emergence of new electronic quantum numbers not present in the atomic case: the projections $\mathbf{\Lambda}$ and $\mathbf{\Sigma}$ of the orbital angular momentum and spin on the internuclear axis. These projections can be defined if the electronic momenta are strongly coupled to the axis and to each other. This case, which implies strong spin-orbit coupling, is called Hund's case (a) (cf. Herzberg 1950). The interaction of the electronic momenta with the rotation of the molecule may cause partial or complete decoupling from the internuclear axis. It is the spin that more often gets decoupled. This case of weak spin coupling is called Hund's case (b). In this case the spin interacts stronger with rotation, and its projection onto the internuclear axis cannot be defined.

Since the magnetic moment of a molecule is determined by the electronic momenta, the expressions for the Zeeman effect depend on which spin coupling case applies. For pure Hund's cases, the expressions for the Landé factors are rather simple, while when the spin is partially decoupled, perturbation calculations are needed (cf. Berdyugina & Solanki 2002).

The Zeeman effect in atomic and molecular lines differ in one fundamental respect. Since molecular rotation contributes to the total angular momentum, $\boldsymbol{J}$ can have values much larger than what is possible in the atomic case, in which only the electronic angular momenta contribute to $\boldsymbol{J}$. As J increases, the relative contribution of rotation to $\boldsymbol{J}$ also increases, while the magnetic moment of the molecule does not change significantly, since the rotational contribution to the magnetic moment is three

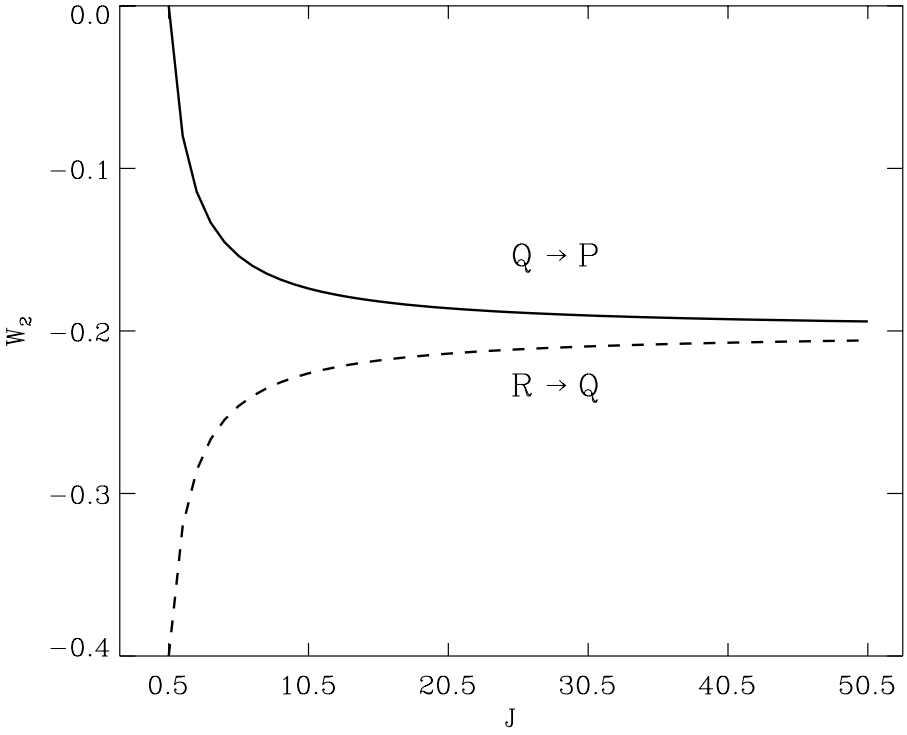

Fig. 3. The intrinsic polarizability W_2 for Raman scattering in molecular lines.

orders of magnitude smaller than the corresponding contribution of the electronic momenta. Therefore the ratio between the magnetic moment of a molecule and its total angular momentum rapidly decreases, which is reflected in the behaviour of the Landé factors.

Below we will consider the electronic transitions of MgH $A^2\Pi - X^2\Sigma$ and C_2 $d^3\Pi - a^3\Pi$, since numerous bands of each have been observed in the photospheric spectrum as well as in the second solar spectrum.

3.1. MgH $A^2\Pi - X^2\Sigma$

Berdyugina & Solanki (2002) have analysed the magnetic properties of this band system in the Zeeman regime (which is relevant also for the present problem) and concluded that the partial decoupling of the spin for the upper electronic state results in significant perturbations of the Zeeman-split rotational levels with $J < 15.5$. The ground state is described by the pure Hund's case (b), since for Σ-states $\Lambda = 0$, and the spin is completely decoupled from the internuclear axis. Note, however, that the coupling of spin with rotation is also not very strong and can easily be destroyed by rather weak external magnetic fields. This would imply a transition to the Paschen-Back regime. For the ground electronic state of MgH, the field strength for which the Paschen-Back effect needs to be taken into account is only 280 G for the very first rotational levels. This value increases with rotation.

In Fig. 4 we give the Landé factors for the doublet rotational levels of the upper and lower states. For the upper state they have been calculated with the perturbation algorithm for partial spin decoupling described by Berdyugina & Solanki (2002). For the lower state they have been computed using the expression for the pure Hund's case (b),

$$g = \frac{1}{J(J+1)} \left\{ \frac{\Lambda^2}{2N(N+1)} \times [\, J(J+1) + N(N+1) - S(S+1)\,] + J(J+1) - N(N+1) + S(S+1) \right\}, \quad (21)$$

and inserting $\Lambda = 0$ for the lower Σ-state. S is the spin quantum number (in our case $S = 1/2$), while N is the quantum number for the total angular momentum excluding spin. N can have the integral values $N = \Lambda, \Lambda+1, \ldots$ (i.e., for the Σ-state $N = 0, 1, \ldots$). The total angular momentum including spin, J, is then formed from N and S as follows: $J = N + S, N + S - 1, \ldots, |N - S|$. Here we thus have $J = N + 1/2$ and $N - 1/2$, which leads to the doublet levels T_1 and T_2. Note that Eq. (21) with $\Lambda = 1$ can also be used to accurately predict Landé factors for the upper, Π-state, levels with $J > 15.5$, for which Hund's case (b) becomes a good approximation.

One can see from Eq. (21) that there is a clear difference between the Zeeman splitting (or Landé factors) of atomic and molecular lines. While the Landé factor of an average atomic line is typically about unity, Landé factors of molecular lines are on average very close to zero (although exceptions exist, see Berdyugina & Solanki 2002). The explanation for this behavior was given in the beginning of this section. In contrast, the probability amplitudes of the Zeeman transitions are identical for the atomic and molecular lines as was concluded in Sect. 2

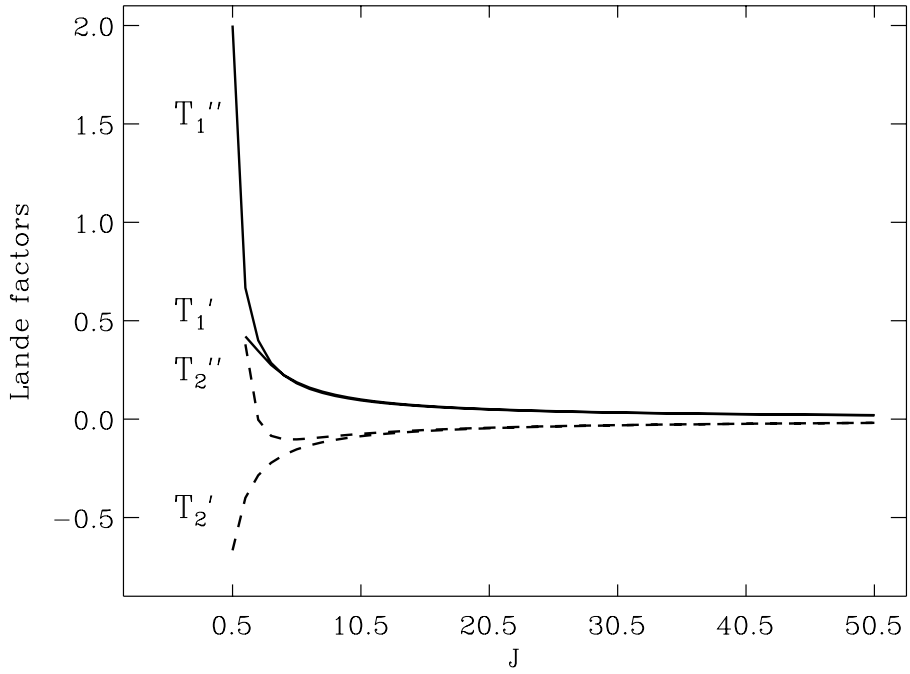

Fig. 4. The Landé factors of the upper and lower multiplet sublevels T′ and T″ of MgH.

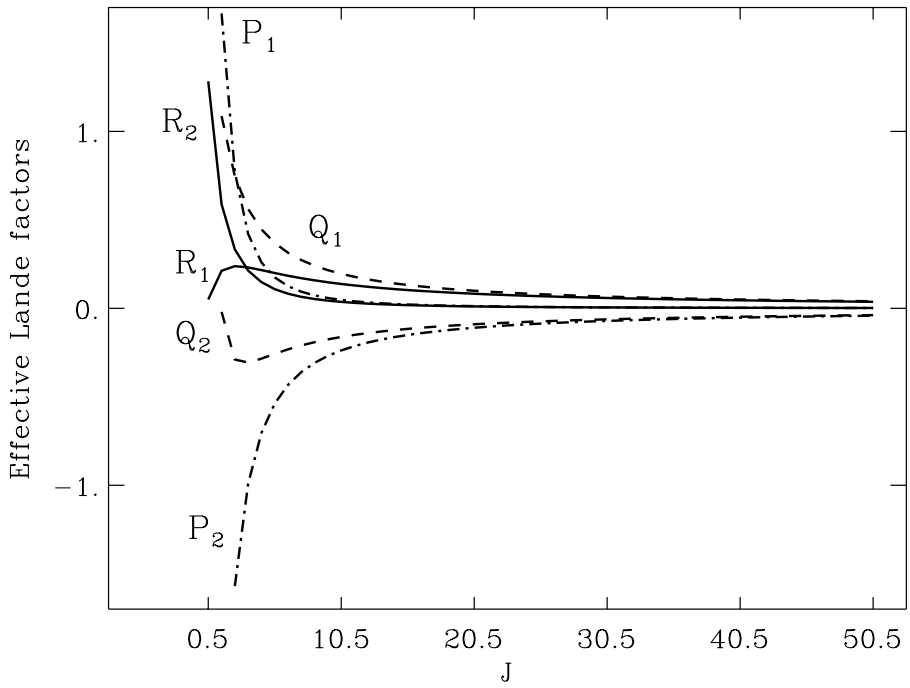

Fig. 5. The effective Landé factors for the rotational branches of the MgH lines: R_1 and R_2 – solid curves, Q_1 and Q_2 – dashed, P_1 and P_2 – dashed-dotted.

(cf. Eq. (8)). The calculation of effective Landé factors for molecular lines is therefore done in the same way as for atomic lines (cf. the expressions in S94, p. 110).

The behaviour of the Landé factors for both states of the MgH green system is that the splitting of the levels becomes independent of J as J increases, while the Landé factors rapidly approach zero (for details, see Berdyugina & Solanki 2002). As a consequence, the effective Landé factors for the very first rotational transitions are the largest, as shown in Fig. 5. The most magnetically sensitive lines are thus excited from the levels with $J < 10.5$. Note also the negative effective Landé factors, which are quite common for molecular transitions (Berdyugina & Solanki 2002).

In the second solar spectrum only MgH lines of the Q_1 and Q_2 branches are observed to be prominent.

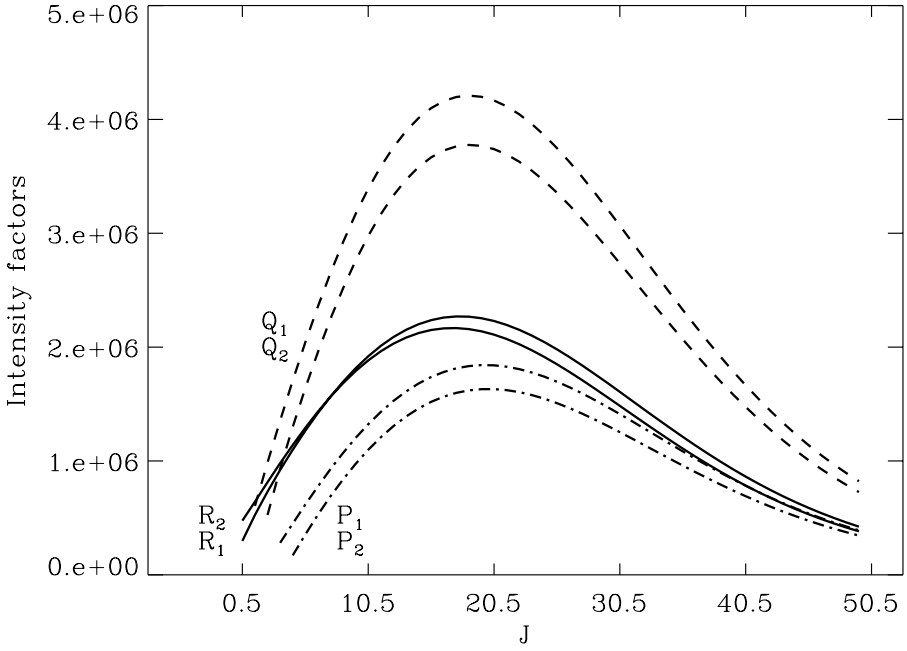

Fig. 6. Same as in Fig. 5, but for the intensity factors of the MgH rotational branches.

To explain this, we have in Fig. 6 calculated for all rotational branches of the $(0,0)$ band the absorption intensity factors defined as follows:

$$I_{J''J'} = f_{J''J'}\,\mathcal{N}_{\max}\,(2J''+1)\exp(-E_{J''}/kT)\,, \qquad (22)$$

where $f_{J''J'}$ is the absorption oscillator strength of the transition $J'' \rightarrow J'$ and $E_{J''}$ is the lower level excitation energy. They were calculated for the intermediate Hund's case (for details, see Appendix) with molecular constants from Bernath et al. (1985) and the $(0,0)$ band oscillator strength, $f_{00} = 0.161$, from Kirby et al. (1979). The calculation has been done with the model of the solar atmosphere by Grevesse & Sauval (1999) for the layer where the number density of MgH reaches its maximum, $\mathcal{N}_{\max}$, where the temperature is $T = 5538\,\mathrm{K}$. This maximum is located well below the temperature minimum because the molecular number density is proportional to the product of the number densities of the atoms that make up the molecules. It is clearly seen from Fig. 6 that the intensity of the Q branches is twice as large as that of the other branches. Combining this with the strong polarizability of the Q branches, we conclude that indeed only these lines should stand out in the observed second solar spectrum. In Table 1 we present their wavelengths (Balfour & Cartwright 1976), polarizabilities W_2, and effective Landé factors g_{eff}.

In our calculations Local Thermodynamic Equilibrium (LTE) and chemical equilibrium have been assumed. It has been shown that these assumptions are valid for molecular opacities in solar and stellar atmospheres, and no deviations from LTE level populations have been found observationally (cf. Johnson 1994). The most significant non-LTE effect on molecular opacities can arise from overionization of neutral atoms, which might reduce the pool from which molecules can be made. This effect will not occur for molecules composed of the abundant elements H, C, N, and O because of their large ionization potentials (11–15 eV). MgH might in principle be affected by overionization of Mg, whose ionization potential is 7.6 eV. The effect is however negligible for the Sun, since the difference in the Mg abundance determined from Mg I and Mg II lines is only 0.05 dex (Lambert & Luck 1978).

3.2. C_2 $d^3\Pi - a^3\Pi$

The magnetic properties of the Swan system of C_2 in the Zeeman regime have been investigated by Berdyugina & Solanki (2002). They concluded that both the upper and lower electronic states of the system are subject to intermediate spin coupling. However, deviations from the pure Hund's case (b) due to incomplete spin decoupling are only seen for small J, while lines with $J \geq 10$ are well described by case (b). Equation (21) can for instance be used for levels with higher J numbers. In general, the magnetic sensitivity of lines from this system is not very large as compared with for instance the MgH band system. The Zeeman regime is appropriate for the C_2 lines up to field strengths as large as 70 kG.

The triplet structure of the C_2 levels is caused by the three different combinations of N and $S = 1$, namely $J = N+1$, N, and $N-1$. They give rise to the three rotational terms T_1, T_2, and T_3. In Fig. 7 we present the Landé factors for the triplet terms of the upper (T') and lower (T'') states. For both states they were calculated using the perturbation algorithm for partial spin decoupling given by Berdyugina & Solanki (2002). The behaviour of the Landé factors is similar to that of the MgH lines, i.e., they are larger for smaller J and rapidly decrease as J

Table 1. Parameters for the Q_1 and Q_2 lines of MgH.

J''	W_2	λ_{Q1}	λ_{Q2}	$g_{\rm eff,\,Q1}$	$g_{\rm eff,\,Q2}$
0.5	0.0000	-	5184.4819	-	-
1.5	0.3200	5186.3727	5184.3126	1.0866	–0.0200
2.5	0.3657	5185.7332	5183.8523	0.7463	–0.2892
3.5	0.3810	5185.0143	5183.2273	0.5609	–0.3069
4.5	0.3879	5184.1583	5182.3579	0.4461	–0.2845
5.5	0.3916	5183.1398	5181.2691	0.3689	–0.2570
6.5	0.3938	5181.9482	5179.9737	0.3138	–0.2317
7.5	0.3953	5180.5798	5178.4786	0.2726	–0.2099
8.5	0.3963	5179.0303	5176.7898	0.2408	–0.1913
9.5	0.3970	5177.2999	5174.9038	0.2155	–0.1754
10.5	0.3975	5175.3807	5172.8340	0.1950	–0.1619
11.5	0.3979	5173.2837	5170.5706	0.1780	–0.1501
12.5	0.3982	5171.0065	5168.1355	0.1636	–0.1399
13.5	0.3985	5168.5523	5165.5185	0.1514	–0.1310
14.5	0.3987	5165.9216	5162.7229	0.1409	–0.1231
15.5	0.3988	5163.1148	5159.7465	0.1317	–0.1161
16.5	0.3990	5160.1327	5156.6007	0.1236	–0.1098
17.5	0.3991	5156.9757	5153.2727	0.1165	–0.1042
18.5	0.3992	5153.6499	5149.7899	0.1101	–0.0991
19.5	0.3992	5150.1427	5146.1369	0.1044	–0.0944
20.5	0.3993	5146.4972	5142.3145	0.0993	–0.0902
21.5	0.3994	5142.6796	5138.3341	0.0946	–0.0863
22.5	0.3994	5138.6959	5134.1963	0.0904	–0.0828
23.5	0.3995	5134.5576	5129.8993	0.0865	–0.0795
24.5	0.3995	5130.2547	5125.4624	0.0829	–0.0765
25.5	0.3996	5125.8119	5120.8574	0.0796	–0.0737
26.5	0.3996	5121.2194	5116.1245	0.0766	–0.0711
27.5	0.3996	5116.4518	5111.2487	0.0738	–0.0687
28.5	0.3996	5111.5989	5106.2258	0.0712	–0.0664
29.5	0.3997	5106.5779	5101.0695	0.0687	–0.0643
30.5	0.3997	5101.4079	5095.8016	0.0664	–0.0623
31.5	0.3997	5096.1549	5090.3683	0.0643	–0.0604
32.5	0.3997	5090.7208	5084.8327	0.0623	–0.0586
33.5	0.3997	5085.1767	5079.1802	0.0604	–0.0570
34.5	0.3998	5079.5260	5073.3960	0.0587	–0.0554
35.5	0.3998	5073.7462	5067.5043	0.0570	–0.0539
36.5	0.3998	5067.8639	5061.5160	0.0554	–0.0525
37.5	0.3998	5061.8697	5055.4115	0.0539	–0.0512
38.5	0.3998	5055.7694	5049.2094	0.0525	–0.0499
39.5	0.3998	5049.5843	5042.8394	0.0512	–0.0487
40.5	0.3998	5043.2974	5036.5337	0.0499	–0.0475
41.5	0.3998	5036.8813	5030.0564	0.0487	–0.0464
42.5	0.3998	5030.4032	5023.4898	0.0475	–0.0454
43.5	0.3998	5023.8432	5016.8471	0.0464	–0.0444
44.5	0.3999	5017.1971	5010.1140	0.0454	–0.0434
45.5	0.3999	5010.4781	5003.3488	0.0444	–0.0425
46.5	0.3999	5003.7019	4996.4895	0.0434	–0.0416
47.5	0.3999	4996.8367	4989.5345	0.0425	–0.0408
48.5	0.3999	4989.9230	4982.3107	0.0416	–0.0399

increases. This is also reflected in the behaviour of the effective Landé factors of the lines shown in Fig. 8.

In the second solar spectrum, only the C_2 lines of the P and R branches are clearly observed, while the lines of the Q branches are missing. Examples of the observed scattering polarization in the P and R branch lines are given in Figs. 9 and 10. This difference with respect to MgH can be understood if line strengths are taken into account. Since in the Swan system both the upper and lower electronic states have the same Λ, i.e., $\Delta\Lambda = 0$, the branches with $\Delta J = 0$, i.e., the Q branches, decrease very rapidly in intensity with increasing J and are therefore most often not observed. This is clearly shown in Fig. 11, where the intensity factors $I_{J''J'}$ for the $(0,0)$ band of the Swan system calculated with Eq. (22) are presented. In this equation, $E_{J''}$ and $f_{J''J'}$ were calculated for the intermediate Hund's case (see appendix) using molecular constants from Huber & Herzberg (1979) and the $(0,0)$ band oscillator strength, $f_{00} = 2.55 \times 10^{-2}$, from Cooper & Nicholls (1976). The calculation was again done with the model of the solar atmosphere by Grevesse & Sauval (1999) for the layer where the number density of C_2 reaches its maximum, where the temperature is $T = 5440\,\mathrm{K}$. We can therefore conclude that C_2 lines of the Q branches are not observed in the second solar spectrum because of their very low transition probabilities. Thus only lines of P and R branches are of interest. In Table 2 we list their wavelengths according to Phillips & Davis (1968), polarizabilities W_2 calculated for the Rayleigh scattering case via Eqs. (15) and (17), and effective Landé factors g.

From Fig. 11 we note that the intensity factors become very small for small values of J. This causes the P and R branch polarization to be very small or practically absent in lines with low J values, as illustrated in Fig. 12 for R branch lines of C_2. The observations thus confirm that the polarization amplitudes scale with the product between the intensity factors and W_2.

It is interesting to note that the polarization observed in the C_2 P and R branch lines is stronger than the polarization in MgH Q branch lines, although, as was shown in Sect. 2.2, the theoretical polarizability of Q lines is on average 4 times larger as compared with P and R lines for any given molecule. This paradox is however resolved if we account for the relative C_2 and MgH intensity factors. Due to the significantly different dissociation energies of C_2 and MgH (6.11 eV and 1.27 eV, respectively), the maximum number density in the solar photosphere is 60 times larger for C_2 than for MgH. The difference is however reduced by the smaller band oscillator strength of C_2: $f_{00}(C_2)/f_{00}(\mathrm{MgH}) = 0.16$. The final ratio of the intensity factors is therefore $I_{J''J'}(C_2)/I_{J''J'}(\mathrm{MgH}) = 9.5$. This is clearly seen from Figs. 6 and 11. When we now account for the factor of four difference in the polarizabilities, we expect that the polarization in the C_2 lines of the solar spectrum should be on average at least twice that of the MgH lines. This conclusion is consistent with the observations.

4. Resolution of the enigma and discussion

With the theoretical tools that we have now developed, we are able to clarify the enigmatic behavior of the molecular lines. The main puzzle, why the molecular lines seem to be immune to the Hanle effect, is resolved by the combination of significant intrinsic polarizability W_2 and very

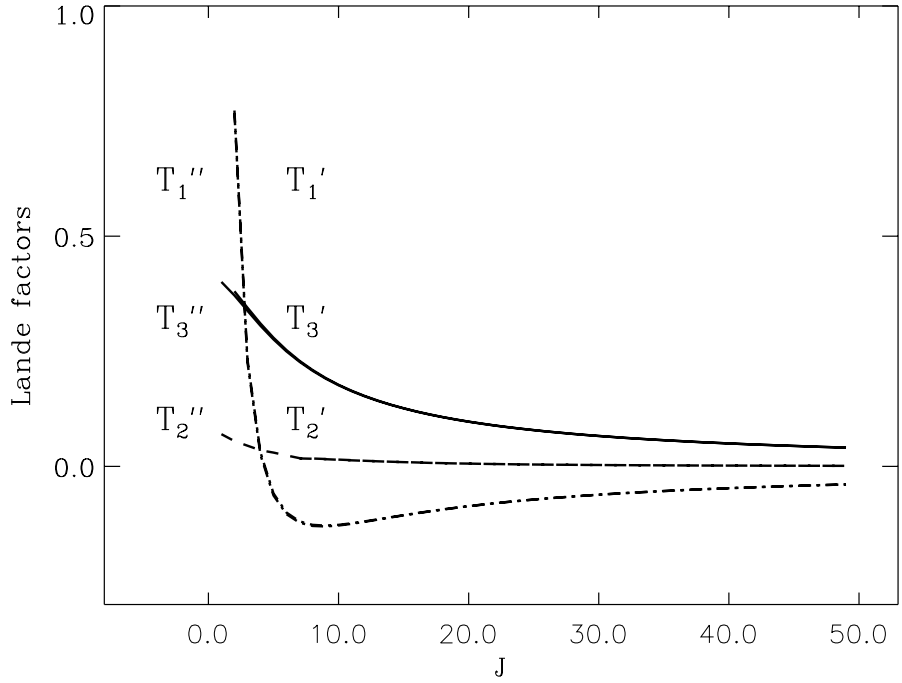

Fig. 7. The Landé factors of the upper and lower multiplet sublevels T′ and T″ of C_2.

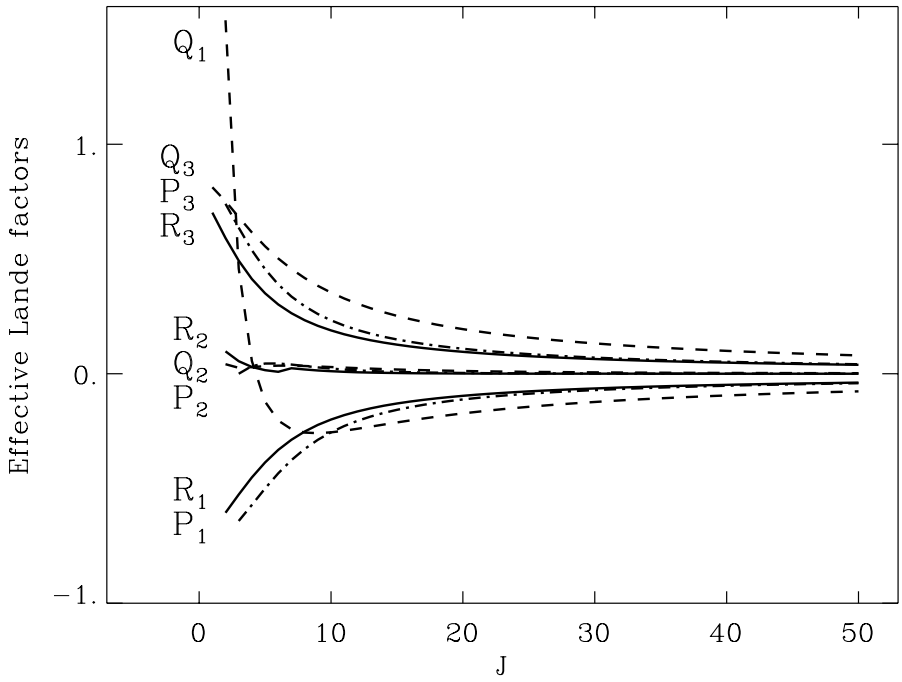

Fig. 8. The effective Landé factors for the rotational branches of the C_2 lines: R branches – solid curves, Q branches – dashed, P branches – dashed-dotted.

small Landé factors. Most molecular lines have, in contrast to most atomic lines, large angular momentum quantum numbers J. When the electron spin S remains small, the Landé factor goes asymptotically to zero as J increases according to Eq. (21).

As molecular transitions with small J are not immune to magnetic fields, it should in principle be possible to observe the Hanle effect for them. However, the intensity factors, which determine the effective strength of the lines as they appear in the solar spectrum, become small when J is small. Since the polarization amplitudes scale with the intensity factors, the lines with significant Landé factors will have vanishing polarization signals. As a consequence all the molecular lines with strong scattering polarization are insensitive to magnetic fields.

The reason why we for MgH only see the Q branch lines in the second solar spectrum is two-fold: (1) the polarizability factor W_2 is four times larger for the Q branch

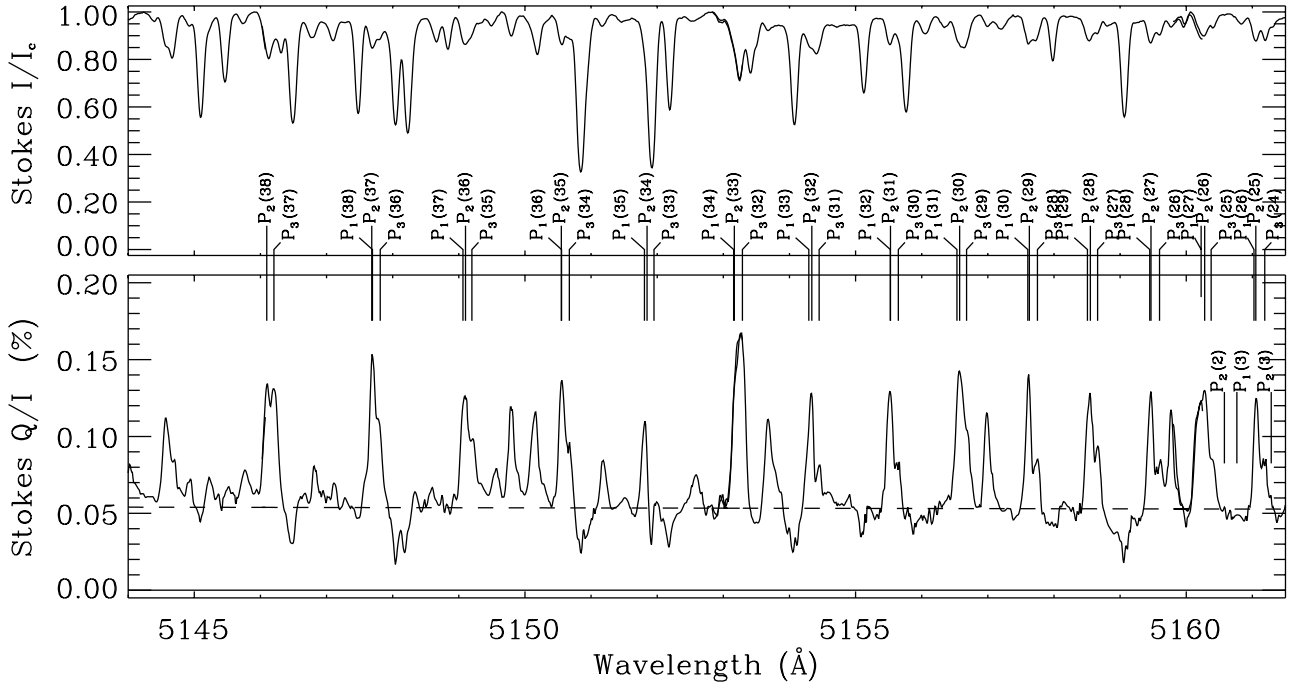

Fig. 9. 17 Å section of the second solar spectrum, from the atlas of Gandorfer (2000) like in Fig. 1, but here illustrating the polarizing molecular lines from the P branch of C_2. The numbers in the brackets are the total angular momentum quantum numbers J for the *lower* level of the transition. Note that while all the lines with high J numbers have prominent polarization peaks, The three lines with small J (2 and 3) marked in the lower right-hand corner of the diagram have no significant polarization. This behavior is explained by Fig. 11 below and in the text.

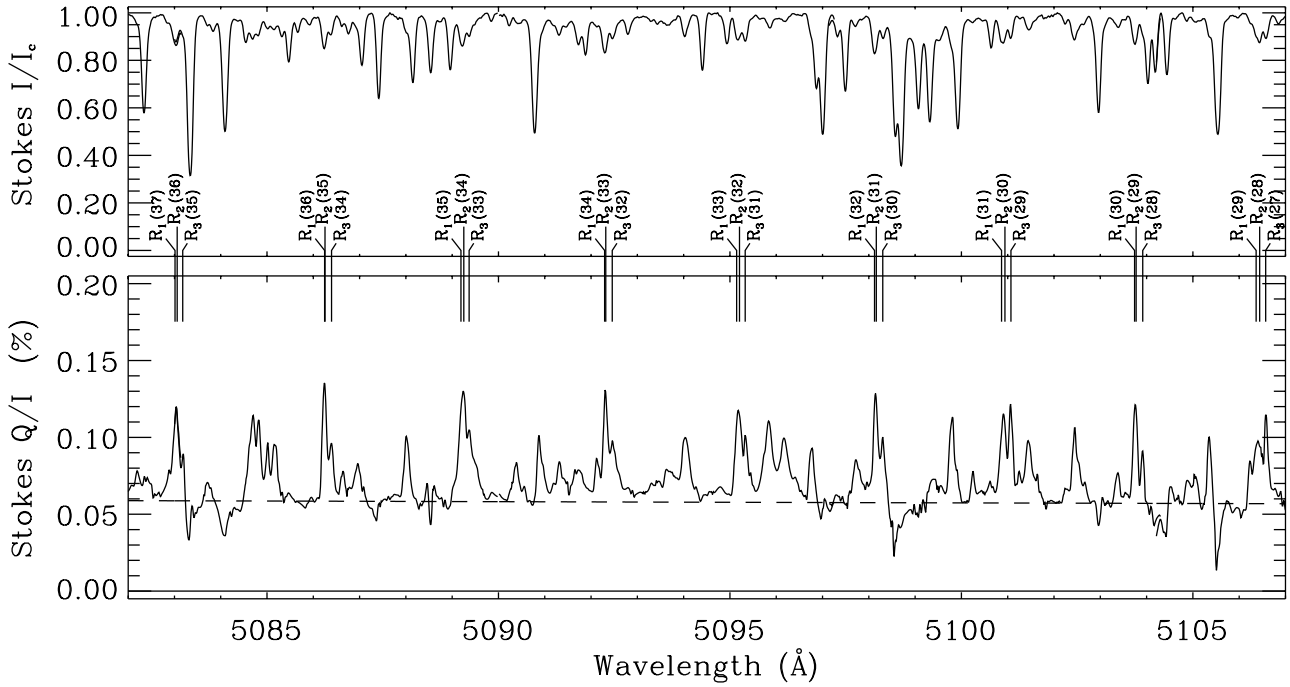

Fig. 10. Similar to Fig. 9, but this time illustrating the C_2 polarization of R branch lines with high J number (given in the brackets for the lower level of the molecular transition).

than for the P and R branches. (2) The intensity factor, which determines the effective line strength, is about twice as large for the Q branch as compared with the P and R branches. The combination of these two factors means that the polarization amplitudes of Q branch lines are expected to be eight times larger than the amplitudes of the P and R branch lines. Therefore only the Q branch lines stand out in the observed spectrum.

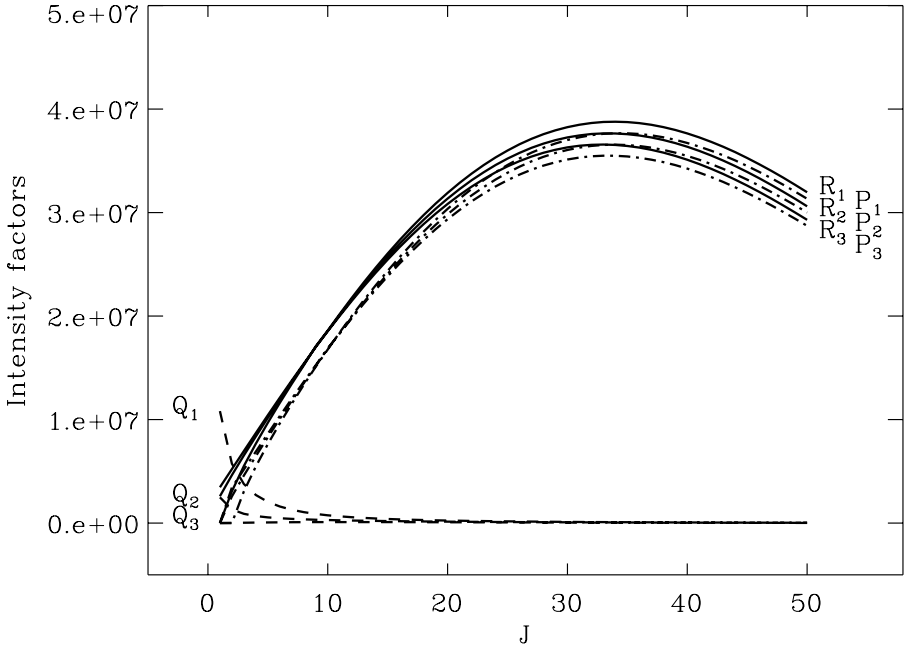

Fig. 11. Same as in Fig. 8, but for the intensity factors of the C_2 rotational branches.

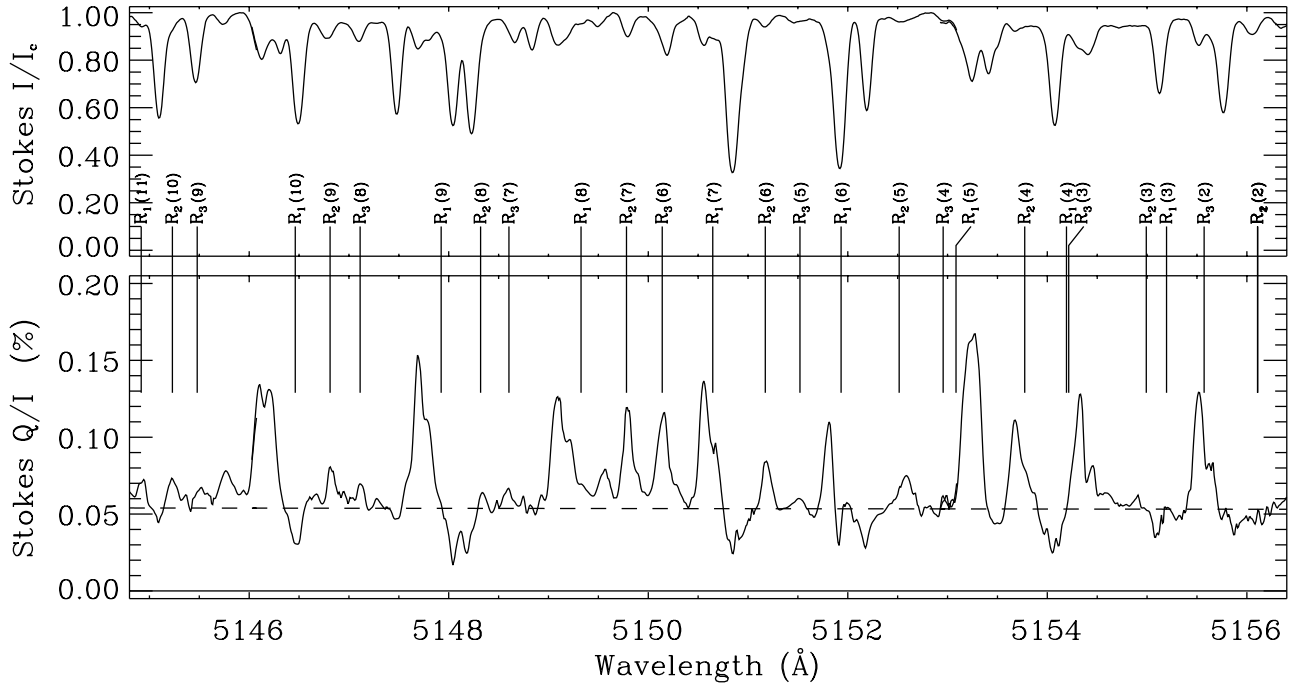

Fig. 12. Same as Fig. 10, but this time for a section of the atlas with R branch lines of C_2 that have small lower-level J values. As expected from the theory these lines have very small or insignificant intrinsic polarization. Note that a substantial part of the spectral range shown here is also covered by the range in Fig. 9. Most of the polarizing lines belong to the P branch lines of C_2. The two polarizing lines near 5150 Å coincide with the locations of two polarizing Q branch lines of MgH ($Q_2(18.5)$ and $Q_1(19.5)$ according to Table 1) and are therefore not evidence for R branch polarization in C_2.

The situation is different for the C_2 lines. Their Q branch lines are missing in the solar spectrum, because they have intensity factors that are almost zero, in contrast to the P and R branch lines. It may seem paradoxical that the observed polarization amplitudes of the C_2 P and R branch lines are often larger than the amplitudes of the MgH Q branch lines, although the intrinsic polarizability W_2 is four times smaller (≈0.1) and the band oscillator strength six times smaller for C_2 than for MgH. Both of these two large factors are however more than compensated for by an even larger factor in favor of C_2: due to the substantially higher dissociation energy for C_2 the number density in the solar atmosphere is about 60 times larger for C_2 than for MgH. When accounting for the difference in

Table 2. Parameters for the P and R branch lines of C_2.

J''	W_2 (P)	λ_{P1} P2 P3	g_{P1} P2 P3	W_2 (R)	λ_{R1} R2 R3	g_{R1} R2 R3
2	0.000	–	–	0.240	5156.108	–0.606
		5160.576	–		5156.108	0.098
		5161.054	–		5155.572	0.591
3	0.014	5160.765	–0.641	0.196	5155.195	–0.526
		5161.285	0.000		5154.992	0.055
		5161.854	0.636		5154.215	0.493
4	0.028	5161.375	–0.572	0.173	5154.192	–0.452
		5161.984	0.033		5153.774	0.029
		5162.578	0.538		5152.956	0.413
5	0.038	5162.037	–0.500	0.159	5153.085	–0.387
		5162.564	0.044		5152.515	0.016
		5163.134	0.456		5151.521	0.350
6	0.046	5162.628	–0.434	0.149	5151.933	–0.332
		5163.134	0.045		5151.173	0.008
		5163.597	0.389		5150.140	0.302
7	0.052	5163.067	–0.376	0.142	5150.647	–0.288
		5163.613	0.040		5149.782	0.024
		5164.095	0.336		5148.604	0.264
8	0.057	5163.537	–0.328	0.137	5149.326	–0.252
		5164.028	0.034		5148.320	0.019
		5164.495	0.294		5147.112	0.233
9	0.061	5163.934	–0.288	0.133	5147.924	–0.223
		5164.371	0.028		5146.811	0.014
		5164.770	0.260		5145.479	0.209
10	0.065	5164.286	–0.255	0.130	5146.462	–0.200
		5164.662	0.023		5145.230	0.011
		5165.013	0.233		5143.860	0.189
11	0.068	5164.559	–0.228	0.127	5144.918	–0.180
		5164.864	0.018		5143.594	0.008
		5165.152	0.210		5142.111	0.172
12	0.070	5164.785	–0.205	0.125	5143.331	–0.164
		5165.028	0.015		5141.891	0.006
		5165.251	0.191		5140.376	0.158
13	0.072	5164.927	–0.187	0.123	5141.645	–0.151
		5165.106	0.012		5140.139	0.005
		5165.252	0.175		5138.505	0.146
14	0.074	5165.029	–0.171	0.121	5139.926	–0.140
		5165.131	0.010		5138.311	0.004
		5165.223	0.161		5136.658	0.136
15	0.075	5165.039	–0.157	0.120	5138.106	–0.130
		5165.080	0.008		5136.437	0.003
		5165.088	0.149		5134.666	0.127
16	0.077	5165.013	–0.146	0.119	5136.270	–0.121
		5164.975	0.007		5134.482	0.002
		5164.939	0.139		5132.693	0.119
17	0.078	5164.892	–0.135	0.118	5134.312	–0.114
		5164.794	0.005		5132.490	0.002
		5164.673	0.130		5130.580	0.112
18	0.079	5164.739	–0.127	0.117	5132.353	–0.107
		5164.551	0.005		5130.411	0.002
		5164.389	0.122		5128.490	0.106
19	0.080	5164.479	–0.119	0.116	5130.266	–0.101
		5164.247	0.004		5128.301	0.001
		5163.989	0.115		5126.253	0.100

Table 2. continued.

J''	W_2 (P)	λ_{P1} P2 P3	g_{P1} P2 P3	W_2 (R)	λ_{R1} R2 R3	g_{R1} R2 R3
20	0.081	5164.201	–0.112	0.115	5128.186	–0.096
		5163.873	0.003		5126.096	0.001
		5163.579	0.109		5124.048	0.095
21	0.082	5163.808	–0.106	0.114	5125.972	–0.092
		5163.440	0.003		5123.874	0.001
		5163.046	0.103		5121.693	0.091
22	0.083	5163.400	–0.101	0.114	5123.781	–0.087
		5162.934	0.002		5121.543	0.001
		5162.511	0.098		5119.374	0.087
23	0.084	5162.871	–0.096	0.113	5121.433	–0.084
		5162.378	0.002		5119.203	0.001
		5161.847	0.094		5116.884	0.083
24	0.084	5162.344	–0.091	0.112	5119.124	–0.080
		5161.734	0.002		5116.751	0.000
		5161.187	0.089		5114.458	0.080
25	0.085	5161.676	–0.087	0.112	5116.652	–0.077
		5161.052	0.002		5114.298	0.000
		5160.377	0.086		5111.847	0.076
26	0.085	5161.024	–0.083	0.112	5114.231	–0.074
		5160.279	0.001		5111.710	0.000
		5159.596	0.082		5109.304	0.074
27	0.086	5160.225	–0.080	0.111	5111.629	–0.071
		5159.467	0.001		5109.154	0.000
		5158.659	0.079		5106.573	0.071
28	0.086	5159.448	–0.077	0.111	5109.093	–0.069
		5158.550	0.001		5106.443	0.000
		5157.750	0.076		5103.917	0.068
29	0.087	5158.506	–0.074	0.110	5106.366	–0.066
		5157.627	0.001		5103.774	0.000
		5156.678	0.073		5101.070	0.066
30	0.087	5157.604	–0.071	0.110	5103.740	–0.064
		5156.573	0.001		5100.940	0.000
		5155.646	0.070		5098.301	0.064
31	0.088	5156.532	–0.069	0.110	5100.867	–0.062
		5155.528	0.001		5098.161	0.000
		5154.449	0.068		5095.330	0.062
32	0.088	5155.525	–0.066	0.109	5098.124	–0.060
		5154.338	0.001		5095.206	0.000
		5153.289	0.066		5092.458	0.060
33	0.088	5154.293	–0.064	0.109	5095.144	–0.058
		5153.166	0.001		5092.317	0.000
		5151.951	0.064		5089.365	0.058
34	0.089	5153.156	–0.062	0.109	5092.292	–0.057
		5151.846	0.001		5089.250	0.000
		5150.672	0.062		5086.394	0.057
35	0.089	5151.807	–0.060	0.109	5089.190	–0.055
		5150.550	0.001		5086.252	0.000
		5149.198	0.060		5083.179	0.055
36	0.089	5150.554	–0.058	0.108	5086.243	–0.054
		5149.101	0.001		5083.059	0.000
		5147.812	0.058		5080.100	0.054
37	0.090	5149.063	–0.057	0.108	5083.013	–0.052
		5147.683	0.000		5079.959	0.000
		5146.204	0.056		5076.763	0.052

oscillator strength we find that the intensity factors for C_2 are larger than those of MgH by a factor of about ten. The observations confirm that the polarization amplitudes do indeed scale not only with the polarizability W_2, but with the product of W_2 with the respective intensity factors.

Recently Faurobert & Arnaud (2002) determined empirical values for the polarizability factor W_2 for nine C_2 lines and two MgH lines in the wavelength range 5157–5161 Å. The determinations were based on observations of the scattering polarization amplitudes just outside the solar limb, where the molecular lines stand out in emission against a weak continuous background spectrum. Off-disk observations have the advantage that dependence of the interpretation on radiative transfer can be avoided, since the emitting layer is optically thin. The disadvantage is however that such observations are notoriously sensitive to stray light, which has a multitude of sources (seeing fluctuations, sky background, instrumental scattering). A large stray light background has to be subtracted from the observations before an interpretation of the spectral features is possible. Based on such observations, Faurobert & Arnaud (2002) find values for W_2 of 0.41 and 0.46 for the two MgH lines, which is in good agreement with the theoretical value of 0.40 according to our Table 1. For the nine C_2 lines, however, they find values spread between 0.13 and 0.26, while according to our Table 2 the theoretically predicted value is 0.09, smaller by approximately a factor of two. It would be important to clarify the nature of this discrepancy, by independent and more extensive observations, as well as by theoretical modelling of the scattering polarization in these lines.

With the theoretical foundation that we have developed here we now have an adequate tool for more systematic explorations and interpretations of the second solar spectrum. Since the intensity factors depend on the physical conditions in the temperature minimum region of the Sun, the absolute values of the polarization amplitudes may be used to diagnose this region. The magnetic invariance of the molecular lines makes them suited to serve as immutable reference lines against which the polarization fluctuations in the atomic lines due to the Hanle effect can be gauged and calibrated. This is of particular importance if one wants to pursue a project to determine the long-term, solar-cycle variations of the Hanle depolarization in atomic lines. By normalizing the polarization scale to the immutable molecular lines, subtle, small drifts that could possibly occur in the polarization scale of the measurements could be eliminated.

Acknowledgements. The observations were carried out with ZIMPOL at IRSOL (Istituto Ricerche Solari Locarno). The engineering group at ETH Zurich (Peter Povel, Peter Steiner, Urs Egger, Frieder Aebersold, Stefan Hagenbuch) built the ZIMPOL system and provided the technical support. The ZIMPOL development program and one of the authors (A.G.) have been funded by the Swiss Nationalfonds, grant no. 20-56853.99. IRSOL receives funding from the canton of Ticino, the city of Locarno, ETH Zurich, and the Swiss Nationalfonds.

Table A.1. Sign of the phase factor for atomic transitions. Here, $\Delta L = L' - L''$ and $\Delta J = J' - J''$.

ΔJ	$(-1)^{r_{J''J'}}$	
	$\Delta L = 0$	$\Delta L = \pm 1$
$+1$	$-$	$+$
0	$\pm^*$	$\pm$
-1	$+$	$+$

* Upper sign for transitions with $J(J+1) \geq S(S+1) - L(L+1)$, lower sign if otherwise.

Appendix A: Sign of the interference terms

A.1. Atomic lines

The sign of the interference terms is determined by the phase factor of the reduced matrix element

$$\begin{aligned}\langle J''||\hat{\boldsymbol{r}}||J'\rangle &= \langle L''SJ''||\hat{\boldsymbol{r}}||L'SJ'\rangle \\ &= (-1)^{L''+S+J'+1} \left\{ \begin{array}{ccc} L'' & L' & 1 \\ J' & J'' & S \end{array} \right\} \\ &\quad \times \sqrt{2J'+1}\sqrt{2L''+1}\,\langle L''||\hat{\boldsymbol{r}}||L'\rangle\,, \end{aligned} \tag{A.1}$$

or, more specifically, by the sign of the product between the first factor on the right hand side (the power of (-1)) and the 6-j symbol (S94, p. 199). This sign is expressed in terms of the parameters r_{ab} and r_{fb} denoted here as $r_{J''J'}$, where J'' and J' are the quantum numbers of the lower and upper levels, respectively (cf. Eqs. (10) and (11)). The sign is given in Table A.1.

A.2. Molecular lines

The sign of the interference terms for molecular transitions is also determined by the phase factor of the reduced matrix element as was concluded in Sect. 2.2. In diatomic molecular spectroscopy uniform and consistent conventions for the electronic transition moments and the rotational line intensities have been formulated by Whiting et al. (1980) following the definition given by Hougen (1970). The expression for the reduced matrix element of a diatomic molecule is known to depend on the way the angular-momentum operators couple to form their resultant, i.e., it is different for different Hund's cases. It has however not been thoroughly discussed whether the phase factor of the molecular matrix elements is sensitive to the angular momentum coupling scheme. Below we present an extended discussion of the subject and try to explain in general physical terms the behaviour of the sign that we derive from the equations.

A.2.1. Hund's case (a)

In Hund's case (a), when the orbital angular momentum and the spin are strongly coupled to each other and to the internuclear axis, they have the projections $\boldsymbol{\Lambda}$ and $\boldsymbol{\Sigma}$, respectively, which together form the total electronic angular momentum about the internuclear axis: $\boldsymbol{\Omega} = \boldsymbol{\Lambda} + \boldsymbol{\Sigma}$

Table A.2. Sign of the phase factor for molecular transitions with Hund's case (a). Here, $\Delta\Omega = \Omega' - \Omega''$ and $\Delta J = J' - J''$.

Branch	ΔJ	$(-1)^{r_{J''J'}}$	
		$\Delta\Omega = 0$	$\Delta\Omega = \pm 1$
R	+1	+	$\mp$
Q	0	+	+
P	−1	+	$\pm$

with quantum numbers $\Omega = |\Lambda + \Sigma|$. Then the total angular momentum $\boldsymbol{J}$ is formed from $\boldsymbol{\Omega}$ and the angular momentum of nuclear rotation, and has quantum numbers $J = \Omega, \Omega+1, \Omega+2, \ldots$ The matrix elements of a diatomic molecule in Hund's case (a) are known expressions (e.g. Hougen 1970; Landau & Lifshits 1963). Here we present them in a more general form, in terms of the rotation group. Thus, if a molecular transition occurs between states described by Hund's case (a), the reduced matrix element is the product of the Clebsch-Gordan coefficient and another reduced matrix element:

$$\begin{aligned}\langle J''||\hat{\boldsymbol{r}}||J'\rangle^{(\mathrm{a})} &= \langle J''\Omega''; 1l|J'\Omega'\rangle\langle v'||\hat{\boldsymbol{r}}||v''\rangle \\ &= (-1)^{J'+\Omega''+1}\sqrt{2J'+1}\begin{pmatrix} J'' & J' & 1 \\ -\Omega'' & \Omega' & l\end{pmatrix} \\ &\quad\times\langle v'||\hat{\boldsymbol{r}}||v''\rangle, \end{aligned} \tag{A.2}$$

where $l = \Omega'' - \Omega'$. The matrix element $\langle v'||\hat{\boldsymbol{r}}||v''\rangle$ represents the amplitude of the transition between vibrational states v' and v'', i.e., it is proportional to the square root of the vibrational band oscillator strength, $\sqrt{f_{v'v''}}$. Note that it is symmetric with respect to the direction of the transition, and it is canceled out when the polarizability of the rotational transition within a given band is calculated. The sign of the interference term in this case is therefore determined by the phase factor of the Clebsch-Gordan coefficient, namely the power of (-1) and the sign of the 3-j symbol. It is given in Table A.2 for different transition types.

The dependence of P and R branch transitions on the sign of $\Delta\Omega$ can be understood if we recall that in a classical interpretation they can be described in terms of linear oscillators that are aligned with the molecular axis and rotate together with it, while $\boldsymbol{\Omega}$ is by definition oriented along this axis. In contrast, transitions in Q branches can be described in terms of oscillators that are perpendicular to the molecular axis, and their sign is not affected by the sign of $\Delta\Omega$. Furthermore, since in Hund's case (a) only transitions with $\Delta\Sigma = 0$ are allowed, it is the sign of $\Delta\Lambda$ that determines the sign of $\Delta\Omega$ and, thus, the sign of the interference term.

A.2.2. Hund's case (b)

In Hund's case (b), when the spin is decoupled from the internuclear axis, the projection $\boldsymbol{\Sigma}$, and thus $\boldsymbol{\Omega}$, is not determined. Therefore, firstly, the total angular momentum excluding spin $\boldsymbol{N}$ is formed from $\boldsymbol{\Lambda}$ and the rotation with quantum numbers $N = \Lambda, \Lambda+1, \Lambda+2, \ldots$, and, secondly, the total angular momentum $\boldsymbol{J}$ is formed from $\boldsymbol{N}$ and $\mathbf{S}$ with quantum numbers $J = N+S, N+S-1, \ldots, |N-S|$. In Hund's case (b) only transitions with $\Delta S = 0$ are allowed. The resulting reduced matrix element for molecular transitions between states described by Hund's case (b) is then

$$\begin{aligned}\langle J''||\hat{\boldsymbol{r}}||J'\rangle^{(\mathrm{b})} &= (-1)^{N''+S+J'+1}\begin{Bmatrix} N'' & N' & 1 \\ J' & J'' & S\end{Bmatrix} \\ &\quad\times(-1)^{N'+\Lambda''+1}\begin{pmatrix} N'' & N' & 1 \\ -\Lambda'' & \Lambda' & k\end{pmatrix} \\ &\quad\times\sqrt{(2J'+1)}\sqrt{(2N'+1)(2N''+1)} \\ &\quad\times\langle v'||\hat{\boldsymbol{r}}||v''\rangle, \end{aligned} \tag{A.3}$$

where $k = \Lambda'' - \Lambda'$. Here again, the reduced matrix element $\langle v'||\hat{\boldsymbol{r}}||v''\rangle$ represents the amplitude of the transition between vibrational states v' and v''. As in Hund's case (a) it divides out when forming the polarizability W_2. The sign of the interference term in this case is thus determined by the power of (-1) and the signs of the 6-j and 3-j symbols. The sign of the first row in Eq. (A.3) is the same as in the atomic case given by Eq. (A.1) with L replaced by N, while the sign of the second row is the same as in Hund's case (a) given by Eq. (A.2) and Table A.2, with Ω and J replaced by Λ and N, respectively.

Table A.3. Sign of the phase factor for molecular transitions with Hund's case (b). Here, $\Delta\Lambda = \Lambda' - \Lambda''$.

Branch	ΔJ	$(-1)^{r_{J''J'}}$	
		$\Delta\Lambda = 0$	$\Delta\Lambda = \pm 1$
R	+1	+	$\mp$
Q	0	$\pm^*$	$\pm^*$
P	−1	+	$\pm$

* Upper sign for transitions with $J(J{+}1) \geq S(S{+}1){-}N(N{+}1)$, lower sign if otherwise.

Here we consider only transitions in the main rotational branches, for which $\Delta J = \Delta N$. Then the resulting signs of the transitions in the R and P branches are the same as in Hund's case (a), while in the Q branches more complicated relations appear (see Table A.3). Taking into account that $J = N+S, \ldots, |N-S|$ for given N and S, the signs of the corresponding Q branch transitions will be positive if $J \geq 0, \ldots, S$. This means that all but the first few Q branch transitions have positive sign as in Hund's case (a).

Let us consider, for example, the MgH $A^2\Pi - X^2\Sigma$ system, for which $S = 1/2$ and $\Delta\Lambda = +1$. The first rotational transitions in the Q_1 and Q_2 branches arise from levels with $J_1 = 1.5$ and $J_2 = 0.5$, respectively, i.e., $N = 1$. The interference term of these transitions is positive, because $S(S+1) - N(N+1) < 0$. This is also valid for all the other transitions in the Q branches.

The resistance of the sign of the interference term in the P and R branches to change between cases (a) and (b) can be explained by the key role played by the sign of $\Delta\Lambda$

(cf. the explanations in Sect. A.2.1), and Λ is a good quantum number for the case (b) coupling scheme. The decoupled spin however tries to affect the sign of the Q branch transitions, which are associated with linear oscillators perpendicular to the molecular axis. The larger the spin value, the more the first transitions are affected, which means that the sign of their interference terms may be changed to become negative.

A.2.3. Intermediate Hund's case (ab)

In the intermediate case between Hund's cases (a) and (b), the spin is only partly decoupled from the internuclear axis. Then the reduced matrix element can only be calculated with perturbation theory. In general it can be expressed in terms of a linear combination of the unperturbed amplitudes, either through $\langle J''||\hat{\boldsymbol{r}}||J'\rangle^{(\mathrm{a})}$ or $\langle J''||\hat{\boldsymbol{r}}||J'\rangle^{(\mathrm{b})}$:

$$\begin{aligned}\langle J''||\hat{\boldsymbol{r}}||J'\rangle^{(\mathrm{ab})} &= \sum_{\Sigma=-S}^{+S} C^{(\mathrm{a})}_{\Sigma,N''} C^{(\mathrm{a})}_{\Sigma,N'} \langle J''||\hat{\boldsymbol{r}}||J'\rangle^{(\mathrm{a})} \\ &= \sum_{\Sigma=-S}^{+S} C^{(\mathrm{b})}_{\Sigma,N''} C^{(\mathrm{b})}_{\Sigma,N'} \langle J''||\hat{\boldsymbol{r}}||J'\rangle^{(\mathrm{b})}, \quad \text{(A.4)}\end{aligned}$$

where $C^{(\mathrm{a})}_{\Sigma,N}$ and $C^{(\mathrm{b})}_{\Sigma,N}$ are the elements of the eigenvectors of the perturbation matrices that transform the case (a) or (b) wavefunctions into the intermediate case wavefunctions. Analytical expressions for $C^{(\mathrm{a})}_{\Sigma,N}$ are given by Kovács (1969) for many electronic states. Practical information on the calculation of perturbation matrices for any electronic states can be found in the recent paper by Berdyugina & Solanki (2002).

Since the sign of the interference term for all the P and R branches and for most transitions in the Q branches are identical for Hund's cases (a) and (b), it is logical that it will conserve its value also in the intermediate case (recalling that Λ is a good quantum number for both cases). Only for the first few transitions in the Q branches detailed calculations are needed. Depending on the value of the spin and on how strongly it is coupled to the internuclear axis, the sign for Q branch transitions may be either positive or negative. These lines are however of very low intensity and are therefore not of practical interest.

Appendix B: Oscillator strengths of molecular lines

According to the convention of Whiting et al. (1980), the absorption oscillator strength of the molecular transition can be expressed via the reduced matrix element considered in Sect. A.2 in the same way as for atomic lines (cf. S94, p. 160):

$$f_{J''J'} = \frac{8\pi^2 m_e \nu_{J'J''}}{3h} |\langle J''||\hat{\boldsymbol{r}}||J'\rangle|^2, \quad \text{(B.1)}$$

where $\nu_{J'J''}$ denotes the energy difference between the upper and lower rotational levels. According to the description given in Sect. A.2, the square of the reduced matrix element in the above expression can be written as a product of two factors. We then obtain

$$\begin{aligned} f_{J''J'} &= \frac{8\pi^2 m_\mathrm{e} \nu_{J'J''}}{3h} |\langle v'||\hat{\boldsymbol{r}}||v''\rangle|^2 \frac{S_{J'J''}}{2J''+1} \\ &= f_{v'v''} \frac{\nu_{J'J''}}{\nu_{v'v''}} \frac{S_{J'J''}}{2J''+1} \quad \text{(B.2)}\end{aligned}$$

where $f_{v'v''}$ is the (v',v'') band oscillator strength, $\nu_{v'v''}$ is the energy difference between the upper and lower vibrational states, and $S_{J'J''}$ is the dimensionless Hönl-London factor. Note that $f_{v'v''}$ and $S_{J'J''}$ are symmetric with respect to the direction of the transition, i.e., they are the same for absorption and emission.

It is clear that the Hönl-London factors are different for different coupling cases. In Hund's case (a), simple analytical expressions can easily be obtained from Eq. (A.2) (they have been tabulated, e.g. by Kovács 1969 and Berdyugina & Solanki 2002). In Hund's case (b), Hönl-London factors for a given electronic transition can also be rather easily expressed via Eq. (A.3), and the final formulae look almost as simple as in Hund's case (a) (cf. Schadee 1969). Analytical expressions for some electronic transitions governed by the intermediate Hund's case (ab) have been obtained by Kovács, but they are rather complicated, and it is more practical to calculate them numerically with the expansion of Eq. (A.4). The normalization of the Hönl-London factors should be done according to the convention of Whiting et al. (1980).

Finally note that for transitions between states with $\Lambda \neq 0$, the lines appear as close doublets because of the Λ-type doubling. The definition of the rotational line strength given by Whiting et al. (1980) implies that a Λ-doublet is composed of two rotational lines. Therefore, if such a doublet is not resolved in the observed spectra, the increase of absorption or emission in the blend is to be accounted for by adding the contributions from two rotational lines whose theoretical strengths are identical.

References

Balfour, W. J., & Cartwright, H. M. 1976, A&AS, 26, 389
Berdyugina, S. V., & Solanki, S. K. 2002, A&A, 385, 701
Bernath, P. F., Black, J. H., & Brault, J. W. 1985, ApJ, 298, 375
Cooper, D. M., & Nicholls, R. W. 1976, Spec. Lett., 9(3), 139
Faurobert, M., & Arnaud, J. 2002, A&A, 382, L17
Feofilov, P. P. 1961, The Physical Basis of Polarized Emission (Consultants Bureau, New York)
Fluri, D. M., & Stenflo, J. O. 1999, A&A, 341, 902
Gandorfer, A. 2000, The Second Solar Spectrum, vol. I: 4625 Å to 6995 Å, ISBN No. 3, 7281, 2764 7 (Zurich: VdF)
Grevesse, N., & Sauval, A. J. 1999, A&A, 347, 348
Herzberg, G. 1950, Molecular Spectra and Molecular Structure. I. Spectra of Diatomic Molecules (Van Nostrand Company, New York)
Hougen, J. T. 1970, The calculation of rotational energy levels and rotational line intensities in diatomic molecules, NBS Mon., 115

Huber, K. P., & Herzberg, G. 1979, Molecular Spectra and Molecular Structure. IV. Constants of Diatomic Molecules (Van Nostrand Reinhold Company, New York)
Ivanov, V. V. 1991, in Stellar Atmospheres: Beyond Classical Models, ed. L. Crivellari, I. Hubeny, & D. G. Hummer (Dordrecht: Kluwer), Proc. NATO, 81
Johnson, H. R. 1994, Molecules in the Stellar Environment, ed. U. G. Jørgensen, IAU Coll. 146, Lect. Notes Phys., 428, 234
Keller, C. U., & Sheeley, N. R. Jr. 1999, in Proc. 2nd SPW, Solar Polarization, ed. K. N. Nagendra, & J. O. Stenflo, ASSL (Dordrecht: Kluwer), 243, 17
Kirby, K., Saxon, R. P., & Liu, B. 1979, ApJ, 231, 637
Kovács, I. 1969, Rotational Structure in the Spectra of Diatomic Molecules, Adam Hilger Ltd., London
Lambert, D. L, & Luck, E. 1978, MNRAS, 183, 79
Landau L. D., & Lifshits, E. M. 1963, Theoretical Physics. III. Quantum Mechanics. Nonrelativistic theory (Fizmatgiz, Moscow)
Phillips, J. G., & Davis, S. P. 1966, The Swan System of the C_2 Molecule and the Spectrum of the HgH Molecule (University of California Press, Berkeley and Los Angeles)
Povel, H. P. 2001, in Magnetic Fields across the Hertzsprung-Russel Diagram, ed. G. Mathys, S. K. Solanki, & D. T. Wickramasinghe, ASP Conf. Ser., 248, 543
Rao, D. M., & Rangarajan, K. E. 1999, ApJ, 524, L139
Schadee, A. 1969, Bull. Astron. Inst. Netherlands, 17(5), 311
Stenflo, J. O. 1994, Solar Magnetic Fields: Polarized Radiation Diagnostics, Astrophysics & Space Science Lib. (Kluwer, Dordrecht), 189 (S94)
Stenflo, J. O. 1998, A&A, 338, 301
Stenflo, J. O., & Keller, C. U. 1996, Nature, 382, 588
Stenflo, J. O., & Keller, C. U. 1997, A&A, 321, 927
Stenflo, J. O., Bianda, M., Keller, C. U., & Solanki, S. K. 1997, A&A, 322, 985
Stenflo, J. O, Keller, C. U., & Gandorfer, A. 1998, A&A, 329, 319
Stenflo, J. O., Gandorfer, A., Wenzler, T., & Keller, C. U. 2001, A&A, 367, 1033
Whiting, E. E., Schadee, A., Tatum, J. B., Hougen, J. T., & Nicholls, R. W. 1980, J. Mol. Spec., 80, 249